

## X-ray imaging techniques on Z using the Z-Beamlet laser

G. R. Bennett<sup>a)</sup>

*Ktech Corporation, Sandia National Laboratories, Mail Stop 1106, P.O. Box 5800, Albuquerque, New Mexico 87185-1106*

O. L. Landen

*Lawrence Livermore National Laboratory, Mailcode L-473, P.O. Box 808, Livermore, California 94550-9234*

R. F. Adams, J. L. Porter, L. E. Ruggles, W. W. Simpson, and C. Wakefield

*Sandia National Laboratories, Mail Stop 1193, P.O. Box 5800, Albuquerque, New Mexico 87185-1193*

(Presented on 20 June 2000)

The Z-Beamlet laser backlighter system at Sandia National Laboratories, which will be operational in 2001, will create a point or area source of high (or moderate) energy x rays behind a Z-accelerator [R. B. Spielman *et al.*, *Phys. Plasmas* **5**, 2105 (1998)]-driven target. In the former case with  $>2$  kJ in up to four pulses of  $<2$  ns total duration in a 20 ns interval, and  $>80\%$  of the  $2\omega$  energy in a  $\sim 50$ - $\mu\text{m}$ -diam focal spot, the resulting  $>4 \times 10^{16}$  W/cm<sup>2</sup> irradiances will generate  $\geq 8.950$ , 8.999 keV (zinc He- $\alpha$ , etc.) x rays. This high-energy source, as either a single point or four separate spots, will be used directly for four-frame point-projection x-ray imaging, and will attain spatial resolutions and signal-to-noise levels significantly better than presently possible on Z using existing methods. In combination with a  $\sim 1$  cm field of view, the technique will be well suited to the large, relatively opaque objects characteristic of Z experiments. This addition is anticipated to have a major impact upon the basic physics of z-pinch implosions, and therefore, possibly the ultimate x-ray powers and hohlraum (vacuum or dynamic) radiation temperatures that may be attainable. Furthermore, in combination with a slightly defocused point source and a medium-energy grazing-incidence microscope, Z-Beamlet may allow various inertial confinement fusion and high-energy-density physics experiments to be studied at even higher spatial resolution and signal-to-noise levels. © 2001 American Institute of Physics. [DOI: 10.1063/1.1315645]

### I. INTRODUCTION

To date, all x-ray imaging diagnostics on the Z accelerator<sup>1-3</sup> at Sandia National Laboratories have relied upon direct self-emission from the accelerator-driven target. For certain experiments, such as time-resolved pinhole imaging of stagnating wire array implosions at low x-ray energies, this is quite sufficient; e.g., Ref. 1. However, although this approach is quite convenient and simple, it does limit one to studies within a restricted temporal window, x-ray energy range, and signal-to-noise level. To this end, the Z facility is presently being upgraded with the addition of a high-power laser, the Z-Beamlet laser backlighter system (Z-Beamlet),<sup>4,5</sup> which will be operational in 2001. This laser will be used primarily as a point-area, high-energy x-ray illumination source (x rays created from laser-plasma interactions with a metallic foil),<sup>6</sup> but will also have the capability of generating x rays over a larger ( $\sim 1$ -mm-diam) area, albeit at moderate 1–3 keV energies. With the laser tightly focused as either a single point or four separate spots onto a backlighter foil, and pulsed at appropriate times, the device would serve as a very high-energy, four-frame, point-projection imaging system. In terms of photon energy, with  $>2$  kJ in up to four pulses of  $<2$  ns total duration in a 20 ns interval, and  $>80\%$  of the  $2\omega$  energy in a  $\sim 50$ - $\mu\text{m}$ -diam spot, the result-

ing  $>4 \times 10^{16}$  W/cm<sup>2</sup> irradiances will generate  $\geq 8.950$ , 8.999 keV x rays (zinc He- $\alpha$ , etc., radiation).<sup>6</sup> Conversely, the large-area source of lower x-ray energy will be used for absorption spectroscopy,<sup>5</sup> or backlighting of a small target imaged with a single, “close-in” pinhole. (Because of the finite spot size, existing pinhole-based imaging devices on Z will not necessarily become any more flexible or useful.)

With Z-Beamlet in the point-area mode, high-energy point-projection radiography—the simplest possible x-ray imaging technique<sup>7</sup>—would appear to be well suited to Z since the objects of interest are generally quite large and opaque. Indeed, this radiography diagnostic is anticipated to have a major impact upon the basic physics of z-pinch implosions, and therefore, possibly the ultimate x-ray powers and hohlraum (vacuum or dynamic) radiation temperatures that may be attainable. However, this imaging technique also has considerable merit for smaller-scale z-pinch investigations. For example, a particularly small-point x-ray source created from an x-pinch plasma has recently contributed to the physics of exploding wire cores in Z-accelerator-like targets.<sup>8</sup> In this vein, for the envisaged Z experiments requiring spatial resolution and signal-to-noise levels higher than possible with the smallest, pinhole-apertured Z-Beamlet point source, there appears to be at least one “x-ray optics” solution. That is, a medium-energy grazing-incidence microscope, in the Kirkpatrick–Baez (KB) configuration,<sup>9</sup> effi-

<sup>a)</sup>Electronic mail: grbenne@sandia.gov

ciently backlit by a slightly defocused Z-Beamlet point source. Although as a trade off the field of view would be considerably smaller, as appropriate for higher resolution and larger magnification, such a device would be required for various inertial confinement fusion (ICF) and high-energy-density physics (HEDP) experiments.

A description of high-energy, four-frame, point-projection imaging with Z-Beamlet, and how it will be implemented on Z, forms the bulk of this article. However, some comments on a single-frame, grazing-incidence KB imager coupled to a four-frame detector are also given. Due to space limitations though, no details of large-area backlighter applications (e.g., absorption spectroscopy and illumination of close-in, single pinholes) are discussed. Instead, emphasis is placed on imaging applications that utilize the point source. Before that, however, a brief description of the Z-Beamlet laser is appropriate.

## II. Z-BEAMLET

With some specific changes to suit the Sandia ICF/HEDP mission, Z-Beamlet is essentially the National Ignition Facility (NIF) prototype laser<sup>10</sup> which operated at Lawrence Livermore National Laboratory (LLNL) during 1995–1998. When complete in 2001, Z-Beamlet will be the second largest ICF/HEDP laser facility in the U.S., and as a backlighter it will have several state-of-the-art features.<sup>4,5</sup> For example, to focus >80% of the  $2\omega$  light into a final spot diameter of  $\sim 50 \mu\text{m}$ , after propagating a 75 m distance to the Z chamber, a 39-actuator deformable mirror will be used. With this adaptive optic located at the front end, the wave front will be corrected at an instant just prior to a full shot, and a near-diffraction-limited focus will be obtained at the transport spatial filter (TSP). Any aberrations beyond this region are expected to be small, and a good TSP focus should result in a tight focal spot on the backlighter foil. Although this system was part of Beamlet at LLNL, the focal-point requirements for Z-Beamlet are somewhat more stringent. Indeed, it is notable that the  $\sim 50\text{-}\mu\text{m}$ -diam focal spot is only  $\sim 6\times$  larger than the  $2\omega$  diffraction limit. That is, if the final lens was truly diffraction limited, then the first zero contour in irradiance (the first zero of the first-order Bessel function of the first kind) would occur at a  $\sim 4 \mu\text{m}$  radius. In terms of some specific additions and deletions to the original Beamlet system, Z-Beamlet will include. (1) Deletion of  $KD^*P$  frequency-tripling crystal; (2) addition of  $2\omega$  relay telescope to transport the beam a 75 m distance to the Z accelerator building; (3) a new master oscillator; and (4) removal of the booster amplifiers. To meet the primary and functional requirements, Z-Beamlet will have the following criteria:

- (1)  $>2$  kJ of  $0.527 \mu\text{m}$  light in a four-pulse picket fence of  $<2$  ns total duration over a 20 ns interval.
- (2) Picket pulse of 0.2–0.5 ns controllable duration.
- (3)  $>80\%$  of energy in a  $50\text{-}\mu\text{m}$ -diam spot (implies an irradiance of  $>4 \times 10^{16} \text{W/cm}^2$ ).
- (4) Ability to insert a phase plate for a smooth, large-area ( $\sim 1$  mm diam) focal spot.
- (5) Ability to create four-point foci, of few mm separation, using a wedged or diffractive optic.

- (6) Ability to point the laser focus along a line perpendicular to, and 0.03–1 m from, the z-pinch axis.

## III. POINT-PROJECTION IMAGING FUNDAMENTALS

The modulation transfer function  $\text{MTF}(f)$ , which conveniently describes the resolution performance of many imaging systems over the entire object plane spatial frequency range,  $0 \leq f < \infty$ , is a suitable tool for understanding Z-Beamlet point-projection imaging. For any near-diffraction-limited application, low-energy point-projection x radiography or otherwise, an accurate MTF description generally includes diffraction effects directly. However, for cases of sufficiently high photon energy this is not strictly necessary, in which case a completely “geometric” analysis often suffices. Indeed, for the point-projection radiography setups envisaged for the Z-Beamlet Z-accelerator system, a geometric description appears to be sufficiently accurate for any of the planned experiment applications. To this end, this section begins with the geometric MTF describing any point-projection imaging system assumed to have negligible diffraction, and then applies it to specific setups designed for Z experiments. Diffraction effects for relevant configuration concludes the discussion.

For an object plane with a sinusoidal intensity of spatial frequency  $f$ , described by

$$\hat{I}_{\text{object}}(f, x) = \frac{1}{2}[1 + \cos(2\pi f x)], \quad (1)$$

the geometric result of point projection at the image plane is

$$\hat{I}_{\text{image}}(f, x) = \frac{1}{2} \left[ 1 + \text{MTF}(f) \cos\left(\frac{2\pi f x}{M}\right) \right], \quad (2)$$

where  $M = (U + V)/U$  ( $M \geq 1$ ) is the system magnification,  $U$  and  $V$  are the point-source-to-target and target-to-image-plane distances,  $a$  is the beam spot radius, and

$$\text{MTF}(f) = \text{sinc}\left(\frac{2\pi f}{M} \frac{V}{U} a\right) = \text{sinc}\left(2\pi f \frac{M-1}{M} a\right). \quad (3)$$

(Equation (3) can be readily derived, but due to space limitations the details are omitted.) For example, a Z-relevant point-projection radiography system of  $2\times$  magnification is shown in Fig. 1, where  $U = V = 1$  m and the “instrument” collection solid angle  $\Delta\Omega$  is  $\Delta\Omega = 0.49 \times 10^{-9}$  sr. These are the distances, and therefore magnification, at which most of the initial Z images will be obtained. From the MTF analytical form [Eq. (3)] a number of interesting points arise, some physically obvious and others not. (a) A near-unitary magnification ( $V \ll U$ ) implies that the spatial resolution approaches infinity (also minimal diffractive degradation would exist); this would be quite impractical, however, since the detector could be destroyed. (b) Similarly, it is evident that  $M = 2$ , while not as effective as near-unitary magnification, is at least preferable to, say,  $M = 10$  (this neglects consideration of the finite detector resolution and diffraction differences). (c) As the beam spot radius  $a$  approaches zero, the spatial resolution tends to infinity. (d) There is no dependence on  $U$  and  $V$ , thus providing  $M$  and  $a$  remain constant any setup can be, say, increased to a larger scale to suit experimental constraints; e.g., detector damage. As a result,

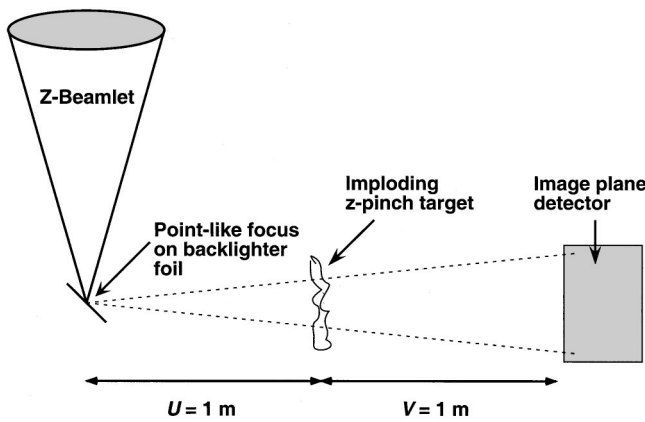


FIG. 1. Standard Z-Beamlet setup for 2× magnification point-projection imaging; i.e.,  $U=V=1$  m. With >80% of the  $2\omega$  laser light focused into a 50- $\mu\text{m}$ -diam spot, 9–12 keV x rays will create a shadow image of the Z-accelerator target at the detector plane. The effective instrument collection solid angle  $\Delta\Omega$  is  $\Delta\Omega=0.49\times 10^{-9}$  sr. To maximize laser–plasma coupling, the backlighter foil normal will be  $<30^\circ$  from the laser line, and not  $45^\circ$  as shown ( $0^\circ$  being normal incidence). Note the irradiance difference between a normally illuminated foil and  $30^\circ$  is  $\sim 0.87$ .

however, diffraction effects will increase and the image brightness will reduce, and visa versa if the system is scaled for a reduction in  $U$  and  $V$ .

As an example of the geometric MTF, the Fig. 1 case of a 50- $\mu\text{m}$ -diam focal spot ( $a=25\ \mu\text{m}$ ) and 2× magnification, implying  $\text{MTF}(f)=\text{sinc}(\pi f a)$ , is shown (solid line) in Fig. 2. Also shown (dashed line) is the degradation effect of increasing the magnification fivefold to 10×, relevant to (b). Note that to maximize laser–plasma coupling, the backlighter foil will be  $<30^\circ$  from the laser line, and not  $45^\circ$  as shown in Fig. 1 ( $0^\circ$  being normal incidence). Therefore, since the analysis so far assumes the point source is circular, it is clear that the effective elliptical emitter will have a different MTF response. Also, the irradiance will be reduced by  $\sim 0.87$  from the normal laser irradiation geometry assumed in the calculation of the  $>4\times 10^{16}\ \text{W}/\text{cm}^2$  irradiance mentioned earlier; i.e., an irradiance of  $>3.5\times 10^{16}\ \text{W}/\text{cm}^2$ . However, to improve spatial resolution beyond that limited by the 50- $\mu\text{m}$ -diam laser spot, 10–25- $\mu\text{m}$ -diam pinholes will routinely be used close to the backlighter foil, as discussed shortly. Hence, it is reasonable to assume that the effective source, as viewed by the detector plane, will generally be quite circular. For Fig. 2, which assumes a circular 50- $\mu\text{m}$ -diam source, one could imagine the laser to be slightly defocused and then apertured along the horizontal line of sight by a 50  $\mu\text{m}$  pinhole. In practice, though, there would be no reason to do this. Anyway, both the 2× and 10× curves of Fig. 2 show repeating, regular zeros (at  $fa=1,2,3,4,\dots$ , for 2× magnification), and a fair amount of the useful spatial frequency with  $\text{MTF}<0$ . This behavior indicates that the image plane sinusoidal pattern has a  $\pi$  phase shift from the input; i.e., phase reversal.

In terms of this example and the analysis so far, it is clear that while the sinusoidal object plane [Eq. (1)] is mathematically very useful, it is in fact rather difficult to obtain in practice. In comparison, a square-wave input from a series of equally spaced opaque bars, is quite trivial to construct, but

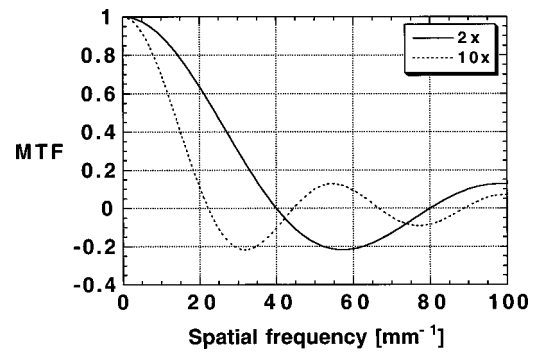


FIG. 2. Geometric modulation transfer function [ $\text{MTF}(f)$ ] for the 2× magnification point-projection radiography setup of Fig. 1 (solid line), except with the assumption that the point source appears circular to the Z target (e.g., the laser spot has been enlarged and a 50- $\mu\text{m}$ -diam pinhole is placed close to the source). Also shown (dashed line) is the response when the magnification is increased to 10×. Note the effective resolution has been reduced, although the larger magnification does at least allow one to better couple the imaging performance to a detector of lesser resolving power; i.e., a gated microchannel plate (MCP). Also note, that  $\text{MTF}(f)$  has repeating, regular zeros, and that when  $\text{MTF}(f)<0$  a phase reversal occurs when mapping from the object to the image plane.

as one may expect has an entirely different form of the MTF. In this regard, since any even, periodic (in  $1/f$ ) function can be constructed from an infinite number of cosine Fourier components, it is intuitive that the new MTF will not act as an overall multiplier. Instead, each Fourier component will have a unique, individual MTF. For example,

$$\hat{I}_{\text{object}}(f,x) = \frac{1}{2} \left( 1 + \frac{4}{\pi} \sum_{n=1}^{\infty} \frac{\sin(n\pi/2)}{n} \cos[n(2\pi f x)] \right) \quad (4)$$

describes an input that is an even square-wave, periodic in  $1/f$ , and the resulting image plane response (output) is

$$\hat{I}_{\text{image}}(f,x) = \frac{1}{2} \left\{ 1 + \frac{4}{\pi} \sum_{n=1}^{\infty} \frac{\sin(n\pi/2)}{n} \times \text{sinc} \left[ n \left( 2\pi f \frac{M-1}{M} a \right) \right] \cos[n(2\pi f x)] \right\}. \quad (5)$$

Note for this more physically obtainable situation, that when  $M=2$  the  $n$ th Fourier MTF component becomes  $\text{sinc}(n\pi f a)$ . Thus, when  $fa=1,2,3,4,\dots$ , the resolution at  $f$  becomes zero; just like the 2× magnification case of Fig. 2. As an example, with  $1/f=a=25\ \mu\text{m}$  the MTF would cross its first zero at  $f=40\ \text{mm}^{-1}$ , and the object plane would correspond to opaque bars 12.5  $\mu\text{m}$  in width, each separated by 12.5  $\mu\text{m}$ .

An object that is even simpler in practice, and one which is particularly straight forward to model the diffraction properties of, is the knife edge. Figure 3 shows the geometric response of the 2× system described in Fig. 2 and the diffraction pattern of a single, infinitely small 9 keV point source. Although the diffraction pattern of only a single point source is shown, it is in fact quite simple to understand the total effect of the 50- $\mu\text{m}$ -diam source. For instance, the area can be considered as an infinite number of uniformly

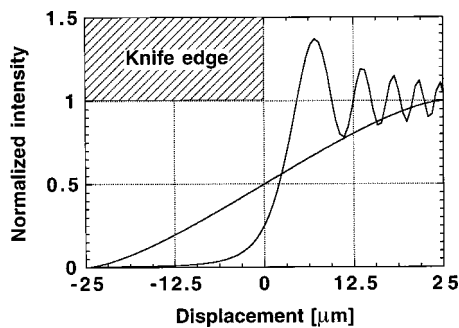


FIG. 3. Geometric knife-edge response of the  $2\times$  system described in Fig. 2, and the corresponding diffraction pattern resulting from an infinitely small point source of 9 keV radiation. From the latter, it is clear that the diffraction distribution from the  $50\text{-}\mu\text{m}$ -diam source, which would be an infinite number of point emitters uniformly distributed over the laser spot area, would not add significant width to the geometric response. For a setup with, say, a  $10\text{-}\mu\text{m}$  source,  $U=0.1111\text{ m}$ , and  $V=1\text{ m}$  for  $10\times$  magnification, i.e., fixed  $V$  but higher magnification, the effects of diffraction are less, as indicated by Eq. (6). Therefore, the geometric response, a spread over  $90\text{ }\mu\text{m}$ , is a better approximation to reality than the  $2\times$  system. Note in the  $10\times$  case that  $\Delta\Omega=0.064\times 10^{-9}\text{ sr}$ , which is a  $\sim 8\times$  reduction from the  $2\times$  system.

distributed point sources generating the same diffraction pattern but at displaced positions on the image plane. Thus, in Fig. 3 it is evident that diffraction would not add significant width to the geometric response. Likewise, for a  $10\times$  system with a  $10\text{-}\mu\text{m}$ -diam source,  $U=0.1111\text{ m}$ , and  $V=1\text{ m}$  (implying  $\Delta\Omega=0.064\times 10^{-9}\text{ sr}$ , an eight-fold reduction over the  $2\times$  magnification configuration), the geometric response for this fixed  $V$ , higher magnification case, is an even better approximation to reality. This is because the blur width added by diffraction would be even less than that of  $2\times$  magnification, but the geometric spread, at  $90\text{ }\mu\text{m}$ , would be larger.

In relation to this, it can be shown that the distance between the  $1/4$  intensity point (knife-edge location) and the peak of the first cycle (approximately the point with a normalized intensity of 1.37),  $\Delta x$ , is

$$\Delta x \approx 1.2\sqrt{\lambda V/2M}. \quad (6)$$

Thus, for the  $2\times$  and  $10\times$  setups,  $\Delta x$  is  $7.04$  and  $3.15\text{ }\mu\text{m}$ , respectively. Therefore, in contrast to purely geometric considerations, this shows that there is an advantage to high magnification. Furthermore, unlike the geometric MTF, there is a dependence on  $V$  and, hence, also on  $U$  for fixed  $M$ .

#### IV. POINT-PROJECTION IMAGING WITH Z-BEAMLET

In the simplest point-projection radiography system on  $Z$ , a four-post picket-fence pulse would allow four separate regions of a target to be imaged at different times [Fig. 4(a)], with up to 20 ns from first to last frame. Using a laser irradiation angle of  $<30^\circ$  on the backlighter foil, the peak irradiance would be  $>3.5\times 10^{16}\text{ W/cm}^2$ . In this case, images of different target locations each at different times would have rather limited value in most experiments. However, the *same* target region could be imaged at different times by using four spatially separated point sources, and the same detector [Fig. 4(b)]. The required several-mm separation of the four-

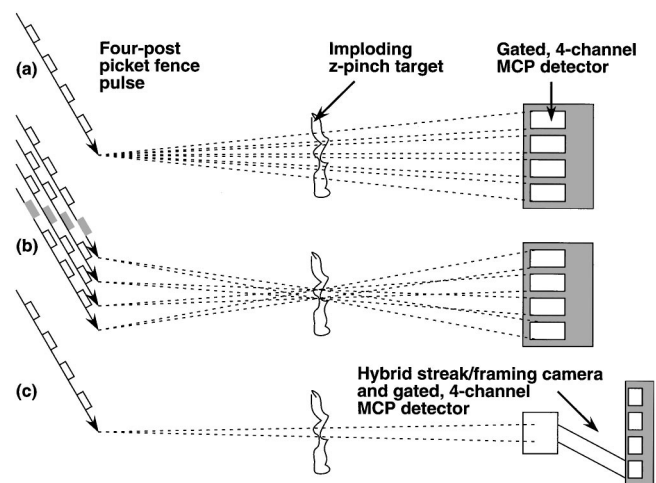


FIG. 4. In the simplest point-projection imaging configuration (a), a four-post picket-fence pulse would allow four separate regions of a  $Z$  target to be imaged at different gated times. The irradiance in this case, at a  $<30^\circ$  laser angle, would be  $>3.5\times 10^{16}\text{ W/cm}^2$ . Alternatively (b), with either a wedged or diffractive optic in the final optic assembly, four spatially separated (of several mm separation) point sources would allow the *same* target region to be imaged at four different gate times. However, although this may be more desirable, it would be obtained at the expense of  $4\times$  laser irradiance reduction to  $>0.88\times 10^{16}\text{ W/cm}^2$ . On the other hand (c), a hybrid streak/framing camera would in principle allow one to obtain four gated frames of the same target region using a single,  $>3.5\times 10^{16}\text{ W/cm}^2$  irradiance point source.

point sources could be obtained by using either a wedged or diffractive optic,<sup>5</sup> and as a trade off the peak irradiance would be reduced by  $4\times$  to  $>0.88\times 10^{16}\text{ W/cm}^2$ . Naturally, this four-fold reduction in irradiance would impact the available x-ray energies. There are, however, two methods to circumvent this problem, which would otherwise waste 75% of the laser energy. The first is to use the same wedged or diffractive optic in the final optic assembly, but split and delay a single laser pulse at the beginning of the amplifier chain. Thus, the square cross-section amplifier profile, split into four equal, independent sections, would amplify each pulse separately. Thereafter, each of the four spatially separated points at the focal plane would only receive one pulse. In which case, the irradiance would be  $>3.5\times 10^{16}\text{ W/cm}^2$  as required. The second possibility would use a hybrid streak/framing camera to capture four gated images from the same target region, illuminated by a single point source [Fig. 4(c)]. Without a spatial multiplexing system and a wedged or diffractive optic, this approach would transfer complexity from the laser to the image plane detector, but it could be the preferred option. Indeed, a hybrid streak/framing camera appears to be the appropriate detector choice for the KB microscope mentioned earlier and discussed shortly.

For the very first point-projection imaging experiments, the overall configuration will initially be that of Fig. 4(a)—four different target regions at different gate times—and the detector will be a four-frame MCP with visible photographic film. The circular active area of each channel will be of 18 mm diam, and the image plane will be 1 m from the  $Z$  target. Likewise, at least for  $2\times$  magnification, the backlighter will be 1 m behind the target. To protect from debris and high-energy bremsstrahlung radiation, the detector will be placed

inside a heavily shielded tungsten box fitted with electromagnetic fast-closing (EMFC) valves. Protecting against debris 1 m from the  $z$  pinch across an 18 mm aperture, is in fact quite a challenge. However, by using electromagnetic gun technology from another Sandia program, the detector box presently has EMFC valves with shutters that approach a 250 m/s velocity. Thus, with two shutters arriving from opposite directions the closing time is  $\sim 36 \mu\text{s}$ , implying debris speeds of  $< 28 \text{ km/s}$  can be guarded against. To put this into perspective, it is interesting to note  $28 \text{ km/s}$  is more than double that of the fastest hypervelocity gas guns used in shock-wave physics applications. Even faster closing times are expected if the valves can be cooled to increase electrical conductivity, however, it is unlikely that the detector would ever be placed closer than 0.8 m from the pinch. Indeed, since the  $2\times$  and  $10\times$  point-projection configurations discussed earlier are essentially dominated by geometric optics (independent of  $U$  and  $V$ , but dependent upon  $M$  and  $a$ ), there would be little reason to reduce  $V$  below 0.8 m, keeping  $M$  fixed, to minimize diffraction. Conversely, an increase in  $V$  beyond 1 m to reduce the risk of debris damage, would be limited by the  $Z$  chamber wall and water insulator on the other side. The same restriction applies to the backlighter-to-target distance  $U$ , at least for the  $2\times$  magnification case of  $U = 1 \text{ m}$ .

In addition to detector enhancements such as a hybrid streak/framing camera for a single point source,  $10\text{--}25\text{-}\mu\text{m}$ -diam pinholes as mentioned earlier will be used to improve spatial resolution beyond that possible with the  $50 \mu\text{m}$  laser spot. (See Ref. 11 for related details concerning pinhole-assisted point-projection radiography on NIF.) In the single point source case, a thick backlighter foil apertured by a nearby pinhole would be preferred over a fiber of  $< 50 \mu\text{m}$  diameter, since it would better withstand multiple pulse irradiation over 20 ns. Furthermore, a fiber could exhibit some radial expansion and, therefore, source broadening. To usefully couple the performance increase to the gated MCP detector, an appropriate increase in magnification beyond  $2\times$  would be required; e.g.,  $10\times$  magnification for a  $10\text{-}\mu\text{m}$ -diam pinhole. Note again from Eq. (3) that the required magnification increase will partially offset the geometric resolution improvement incurred from the spot size reduction. However, it would reduce the small diffraction degradation, as implied by Eq. (6). The most obvious disadvantage to improving resolution in this way is the reduction in the instrument collection solid angle  $\Delta\Omega$ . For example, the  $10 \mu\text{m}$  source relevant to the  $10\times$  setup mentioned earlier has  $\Delta\Omega = 0.064 \times 10^{-9} \text{ sr}$ . Similarly, a  $5 \mu\text{m}$  pinhole and  $20\times$  magnification ( $U = 0.0526 \text{ m}$  and  $V = 1 \text{ m}$ ) has  $\Delta\Omega = 0.018 \times 10^{-9} \text{ sr}$ . With a  $27\times$  reduction in  $\Delta\Omega$  from  $50 \mu\text{m}$  ( $M = 2$ ) to  $5 \mu\text{m}$  ( $M = 20$ ), it is apparent that there is a natural penalty in obtaining higher resolution. (Note, for temporally streaked, one-dimensional imaging, where the spot needs to be small in only one dimension, a pin slit could replace a pinhole so that the effective brightness would be larger.) A less certain disadvantage, is the possibility that a  $5 \mu\text{m}$  pinhole 53 mm from the pinch could “close” during the tens of ns that it would be bathed in “run-in” radiation during the pinch implosion. To this end, the following section describes

one possible “x-ray optics” option for reliably obtaining high resolution with good collection efficiency, at lower energy and over a smaller field of view. Before that and as an aside, it is interesting to note that point-projection radiography is, in fact, very efficient compared to, say, area backlit pinhole imaging where the actual collection solid angle may be the *same*. This is because in the latter, the laser energy has to be distributed over an area larger than the object being imaged; whereas, in the former the energy can be concentrated into a small spot while still fully illuminating a large object.

## V. HIGH-ENERGY GRAZING-INCIDENCE IMAGING WITH Z-BEAMLET

To obtain higher resolution than possible with point-projection imaging, it is clear that an x-ray optic imaging device would have to use Z-Beamlet in either the point- ( $\sim 50 \mu\text{m}$  diam) or area-source ( $\sim 1 \text{ mm}$  diam) mode. However, because the imager could be required to study ICF implosions, for example, where the capsule size, at least initially, is  $\sim 2 \text{ mm}$  in diameter, it is already clear that pinhole imaging would not be possible with even the  $1 \text{ mm}$  laser spot. Furthermore, high-resolution applications requiring high x-ray energies, and therefore, the  $50 \mu\text{m}$  laser spot, would compound the problem much further. However, in addition to point-projection radiography, one of at least two other imaging techniques that could image an object larger than the backlit illumination area is the approach based on curved crystals.<sup>12</sup> Radiography systems of this type have been very successful, particularly on the Nike Laser at the Naval Research Laboratory, and a spherical concave quartz crystal has achieved  $\sim 1.7 \mu\text{m}$  resolution at  $1.473 \text{ keV}$ .<sup>12</sup> Due to a number of issues, however, it will not be possible to field a high-resolution, and therefore, high-magnification, curved crystal imager on  $Z$  other than at  $M \sim 1\text{--}2$ . In terms of a near-horizontal view from one of the main  $12^\circ$  diagnostic lines of sight (LOS) approximately perpendicular to the vertical pinch, the placement of a crystal behind the target will be precluded by the disk-shape magnetically insulated transmission lines [(MITLs), see Fig. 1 of Ref. 1]. Likewise, an axial view will also be obstructed by the MITLs, although in either case appropriate modifications to  $Z$  could overcome these problems. On the other hand, an appropriately designed KB microscope could both be fielded on  $Z$  without requiring any changes to the power flow hardware, *and* image an object larger than the backlighter area, as required. For instance, a KB device could be located axially below the  $Z$  target and backlit from above. However, as with a curved crystal imager, a near-horizontal view in a  $12^\circ$  LOS would not be possible.

In terms of existing KB microscopes used in ICF applications, the numerical aperture (NA) has generally been “defined” by the full mirror area.<sup>13</sup> Thus, the same mirror surface is used for all points of the object plane, and as a result, the backlighter area (if a backlighter is used) is at least as large as the object being imaged. However, by using a suitably located aperture stop behind an oversized KB mirror pair, it is possible to effectively employ a different mirror

section for each object plane point. In addition to a likelihood of improved spatial resolution performance, via a reduction of off-axis geometric aberrations,<sup>14</sup> a correct stop location can beneficially change the direction that the illuminating rays appear to come from. Specifically, the stop location can be adjusted until the rays effectively emerge from a backlighter area that is smaller than the target object, as required. Indeed, without going into detail, it would be possible—using sufficiently long mirrors—to effectively illuminate a 2-mm-diam capsule with only a slightly defocused Z-Beamlet point source of, therefore, relatively high x-ray energy. For example a  $\sim 300\text{-}\mu\text{m}$ -diam spot, implying a  $\sim 1 \times 10^{15}\text{ W/cm}^2$  irradiance, could generate copious quantities of 4.295, 4.316 keV scandium He- $\alpha$  x rays. In regards to a suitable image plane detector for a single-frame KB of this type, a hybrid streak/framing camera would be appropriate [Fig. 4(c)].

## VI. SUMMARY AND DISCUSSION

In summary, the Z-Beamlet laser backlighter system, which will be operational in 2001, will be used primarily as a high-energy point-projection x-radiography system for imaging Z-accelerator-driven targets. In combination with the inherently large  $\sim 1$  cm field of view and  $>9$  keV x-ray energies, the imaging technique will be well suited to the large, relatively opaque objects characteristic of Z. Therefore Z-Beamlet will be a critical addition to existing, pinhole-based x-ray imaging diagnostics that rely on self-emission alone, and have limited spatial resolution. Indeed, it is expected that this enhancement will have a major impact upon z-pinch physics, and perhaps the ultimate x-ray powers and hohlraum radiation temperatures that may be possible on Z and future accelerators. With a  $\sim 50\text{-}\mu\text{m}$ -diam focal spot containing  $>80\%$  of the  $2\omega$  energy, Z-Beamlet will allow four-frame imaging with  $\sim 0.2\text{--}0.5$  ns gate times over a 20 ns interval. Using this spot in a  $2\times$  magnification configuration with  $U=V=1$  m, the resulting performance is, to a reasonable approximation, dominated by geometric optics. Likewise, for higher-resolution applications, a pinhole-assisted setup with a  $10\ \mu\text{m}$  spot,  $U=0.1111$  m, and  $V=1$  m for  $10\times$  magnification, has even less diffractive degradation.

In regards to the highest-resolution applications, point-projection imaging with a  $5\ \mu\text{m}$  pinhole—to limit the laser focal spot—may be about the smallest point source that is reasonable. This is because the required high magnification of, say,  $20\times$  would imply a pinhole-to-pinch distance of  $\sim 53$  mm (an increase in  $V$  beyond 1 m to help attain  $20\times$  magnification would amplify diffractive degradation). Thus, at such a short distance the pinhole would be bathed in radiation during the pinch implosion, and the hole could close

prior to the event of interest. To this end, the requirement for an x-ray optics solution to high resolution is apparent. Given that a single, close-in pinhole backlit with the 1 mm laser spot would have insufficient field of view for the applications of interest, this led to the consideration of two options that could image an object larger than the Z-Beamlet focal spot. However, the first of these, a curved crystal imager, was discounted as only a low-magnification system could be fielded on Z without otherwise incurring power flow hardware changes. Nevertheless, the importance and impact of such systems when appropriately accommodated should not be forgotten. Conversely, a suitably designed KB microscope using a correctly located aperture stop could both be fielded on Z, and image an object larger than the laser spot. For example, with sufficiently long mirrors it would be possible to illuminate a 2-mm-diam capsule using only a slightly defocused Z-Beamlet point source. Retaining a fairly small focal spot implies that relatively high x-ray energy can still be generated, even though the peak irradiance is less than the  $50\ \mu\text{m}$  case. As with point-projection radiography, the ability here to use a small laser spot for illuminating a large object, allows high-energy x rays to be generated and at the same time increases the effective collection efficiency.

## ACKNOWLEDGMENTS

This work was performed under the auspices of the United States Department of Energy by Sandia National Laboratories under Contract No. DE-AC04-94AL85000, and Lawrence Livermore National Laboratory under Contract No. W-7405-ENG-48. Sandia is a multiprogram laboratory operated by Sandia Corporation, a Lockheed Martin Company.

<sup>1</sup>R. B. Speilman *et al.*, Phys. Plasmas **5**, 2105 (1998).

<sup>2</sup>M. K. Matzen, Phys. Plasmas **4**, 1519 (1997).

<sup>3</sup><http://www.sandia.gov/pulspowr/hedief/> Pulsed Power ICF Program; Sandia National Laboratories: home page

<sup>4</sup><http://www.z-beamlet.sandia.gov/>

<sup>5</sup>Lawrence Livermore National Laboratory unclassified Report No. UCRL-ID-129722 (1998).

<sup>6</sup>David Attwood, *Soft X rays and Extreme Ultraviolet Radiation: Principles and Applications* (Cambridge University Press, Cambridge, UK, 2000).

<sup>7</sup>T. A. Shelkovenko, S. A. Pikuz, A. R. Mingaleev, and D. A. Hammer, Rev. Sci. Instrum. **70**, 667 (1999); *ibid.* (these proceedings).

<sup>8</sup>S. A. Pikuz, T. A. Shelkovenko, D. B. Sinars, J. B. Greenly, Y. S. Dimant, and D. A. Hammer, Phys. Rev. Lett. **83**, 4313 (1999); Rev. Sci. Instrum. (these proceedings).

<sup>9</sup>P. Kirkpatrick and A. V. Baez, J. Opt. Soc. Am. **38**, 766 (1948).

<sup>10</sup>Bruno M. Van Wonterghem *et al.*, Appl. Opt. **36**, 4932 (1997).

<sup>11</sup>A. B. Bullock, O. L. Landen, and D. K. Bradley, Rev. Sci. Instrum. (these proceedings).

<sup>12</sup>Y. Aglitsiy, T. Lehecka, S. Obenschain, C. Pawley, C. M. Brown, and J. Seely, Rev. Sci. Instrum. **70**, 530 (1999); *ibid.* (these proceedings).

<sup>13</sup>F. J. Marshall, M. M. Allen, J. P. Knauer, J. A. Oertel, and T. Archuleta, Phys. Plasmas **5**, 1118 (1998).

<sup>14</sup>G. R. Bennett, Rev. Sci. Instrum. **70**, 608 (1999).